CrossMark

ORIGINAL PAPER

Comparative physical and chemical analyses of cotton fibers from two near isogenic upland lines differing in fiber wall thickness

Hee Jin Kim · Christopher M. Lee · Kevin Dazen · Christopher D. Delhom · Yongliang Liu · James E. Rodgers · Alfred D. French · Seong H. Kim

Abstract The thickness of cotton fiber cell walls is an important property that partially determines the economic value of cotton. To better understand the physical and chemical manifestations of the genetic variations that regulate the degree of fiber wall thickness, we used a comprehensive set of methods to compare fiber properties of the immature fiber (*im*) mutant, called immature because it produces thin-walled fibers, and its isogenic wild type Texas Marker-1 (TM-1) that is a standard upland cotton variety producing normal fibers with thick walls. Comprehensive structural analyses showed that *im* and TM-1 fibers shared a common developmental process of cell wall thickening, contrary to the previous report that the phase in the *im* fiber development might be retarded. No significant differences were found in cellulose content, crystallinity index, crystal size, matrix polymer composition, or in ribbon width between the isogenic fibers. In contrast, significant differences were detected in their linear density, cross-section micrographs of fibers from opened bolls, and in the lateral order between their cellulose microfibrils (CMFs). The cellulose mass in a given fiber length was lower and the CMFs were less organized in the *im* fibers compared with the TM-1 fibers. The presented results imply that the disruption of CMF organization or assembly in the cell walls may be associated with the immature phenotype of the *im* fibers.

Keywords Cellulose microfibrils · Cotton fiber thickness · Fiber maturity · Immature fiber (*im*) mutant · Plant cell wall · Sum frequency generation (SFG) spectroscopy

H. J. Kim (✉)
Cotton Fiber Bioscience Research Unit, Southern Regional Research Center, USDA-ARS, 1100 Robert E. Lee Blvd., New Orleans, LA 70124, USA
e-mail: heejin.kim@ars.usda.gov

C. M. Lee · K. Dazen · S. H. Kim (✉)
Department of Chemical Engineering, Materials Research Institute, Pennsylvania State University, University Park, PA 16802, USA
e-mail: shkim@engr.psu.edu

C. M. Lee · S. H. Kim
Center for Lignocellulose Structure and Formation, The Pennsylvania State University, University Park, PA 16802, USA

C. D. Delhom · Y. Liu · J. E. Rodgers · A. D. French
Cotton Structure and Quality Research Unit, Southern Regional Research Center, USDA-ARS, 1100 Robert E. Lee Blvd, New Orleans, LA 70124, USA

Introduction

Cotton (*Gossypium* sp.) is the world's most economically important natural fiber (Wakelyn et al. 2010). Botanically, cotton fibers are single trichome cells that normally have a thick secondary cell wall (SCW) composed of almost pure cellulose (Haigler 2010; Kim and Triplett 2001). During cotton fiber development, genes involved in SCW biosynthesis are up-regulated around 14–16 days post anthesis (DPA) and cellulose content in developing fibers dramatically increases. During the fiber wall thickening stage (17–33 DPA), the rate of fiber elongation decreases, whereas the degree of fiber wall thickness increases as the β-1,4-glucan chains form the highly ordered structures called cellulose microfibrils (CMFs) and are packed in the SCW. CMFs are arranged helically around the growing fiber with periodic reversals in the deposition angle. Fibers become twisted due to these reversal regions (Haigler 2010; Kim and Triplett 2001). The orientation of CMFs in developing fiber correlates with fiber strength (Moharir 1998; Moharir et al. 1999). After 40–60 DPA depending on genotype and environmental condition, cotton fibers do not develop further. Mature fibers mainly consist of cellulose Iβ that is mostly found in higher plants (Atalla and Vanderhart 1984).

Upland cotton is a polyploid cotton species (*Gossypium hirsutum* L.) and comprises greater than 90% of world cotton production (Zhang et al. 2008). Texas marker-1 (TM-1) is a standard cultivated upland cotton variety extensively used for genetic and genomic studies (Kohel et al. 1970; Li et al. 2015; Zhang et al. 2015). A cotton mutant named immature fiber (*im*) was originally identified from an upland cotton variety Acala 4–42 (Kohel et al. 1974). Under normal environmental conditions, the *im* plants produce non-fluffy cotton bolls with immature fibers, whereas wild type TM-1 plants produce fluffy cotton bolls with mature fibers (Fig. 1). Phenomenologically, the *im* cotton bolls appear similar to non-fluffy tight lock bolls produced by the wild type cotton plants grown under severe stress conditions. By back-crossing the original *im* mutant several times with the wild type TM-1, the near isogenic lines (NILs) differing in fiber maturity were developed (Kohel and McMichael 1990). The fiber maturity representing the degree of fiber cell wall thickness is often indirectly estimated as "micronaire (MIC)", values of which are determined by measuring air-flow resistance of a certain weight of cotton fibers. Due to the difference of fiber maturity, the MIC value of *im* fibers is significantly lower than that of TM-1 fibers. Thus, it was previously assumed that SCW cellulose biosynthesis responsible for cotton fiber maturity might be arrested or retarded during *im* fiber development (Percy et al. 2015). The NILs have been suggested as a model system for studying SCW cellulose biosynthesis and cotton fiber maturity (Benedict et al. 1999).

Recent studies showed that the *im* fibers were indeed composed of thinner fiber walls than the TM-1 fibers (Kim et al. 2013a) and the *im* gene dysregulated stress-responding genes (Kim et al. 2013b). Genetic studies showed that the *im* gene is located at chromosome 3 and is identified with a recessive, single-locus genetic lesion (Kim et al. 2013a; Kohel et al. 2002; Wang et al. 2013). A fine-mapping analysis has shown that a frame-shift deletion in a mitochondria targeted pentatrico-peptide repeat (PPR) gene is linked to the *im* phenotype (Thyssen et al. 2016). Despite the extensive lists of genes that are differentially expressed between the NILs, their functions have not been well characterized partially due to lack of accurate phenotypic information of the NIL fibers.

To better understand the mechanisms that regulate fiber wall thickness and to bridge the gap between genotypic and phenotypic approaches, we compared physical and chemical properties of developing and fully developed fibers from these NILs using fiber-specific methods that are used in cotton industries to determine cotton quality and value as well as general and advanced laboratory methods. Fiber-specific evaluations included gravimetric fineness, and measurements with a High-Volume Instrument (HVI), an Advanced Fiber Information System (AFIS), and a Cottonscope®. General laboratory methods were a wet-chemical assay for cellulose, cross-sectional image analysis microscopy [IAM], and polarized optical microscopy of longitudinal fiber arrays. Advanced analytical methods included Raman, Fourier Transform Infrared (FTIR), and sum-frequency-generation (SFG) spectroscopy as well as X-ray powder diffraction (XRD). These comprehensive analyses showed that there are common developmental processes and structural similarities between *im*

Fig. 1 Comparisons of fully developed cotton bolls from two near isogenic upland cotton lines. Wild type Texas Marker-1 (TM-1) shows fluffy bolls, whereas the immature fiber (*im*) mutant shows non-fluffy bolls

TM-1   *im*

and TM-1 but there are clear differences of CMF packing within the fiber cell walls.

Experimental

Materials and sample preparation

Two cotton NILs, TM-1 and *im*, were grown in a field of USDA-ARS in New Orleans, LA in 2011. Cotton flowers were tagged at day of anthesis (0 days post anthesis [0 DPA]). Two biological replicates of the NIL fibers were harvested at 10, 17, 24, 28, 33, 37, and 48 DPA. The developing fibers (10–37 DPA) from 10–30 ovules from fifty plants were manually cut from the seeds for each biological replication. These fibers were dried at 40 °C for 2 days . The fully developed fibers (48 DPA) were harvested after the bolls opened naturally at 42–44 DPA and the fibers became mature in the cotton field (Kim 2015). Fibers were removed from the cottonseed using a laboratory roller gin. The two NILs were grown side by side and were treated equivalently and at the same time during planting, tagging, harvesting, and ginning. Standard conventional field practices were applied during the growing season. The soil type in New Orleans was Aquent dredged over alluvium in an elevated location to provide adequate drainage.

Fiber property measurements

Before measurement, all fibers were pre-equilibrated at 65% humidity and 21°C for 48 h. Averages of five

tests were determined in the Cotton Fiber Testing Lab in the USDA-ARS-SRRC located in New Orleans, LA. Physical properties of fibers including Micronaire (MIC), maturity index, Upper-Half Mean Length (UHML), strength (g/tex), and elongation (%) were measured by an HVI (USTER Technologies Inc., Charlotte, NC) that is defined as a standardized instrument for testing cotton by the International Cotton Advisory Committee (ICAC). Standard cotton fibers obtained from USDA-AMS were used to calibrate the HVI according to the manufacturer's instructions. Maturity ratio (MR) and fineness were measured by an Uster® AFIS-Pro (USTER Technologies Inc., Knoxville, TN). The average AFIS fiber data were obtained from five replicates with 5000 fibers per replicate. The AFIS is included in quarterly international round trials under a service agreement, and is routinely examined twice a year by an Uster technician, including maturity measurements. Gravimetric fiber fineness was directly measured as mass per unit length, and reported as millitex (mtex) that is milligrams per kilometer of fibers (ASTM standard D1577-07 2012b). The weights of 300 fibers that were combed and cut at the top and bottom to leave 15 mm lengths from the NILs were measured by a microbalance. Average gravimetric fineness was calculated from the three measurements.

Cellulose assay

Cellulose content in cotton fibers at each developmental stage was measured by the method described by Updegraff (1969) with minor modifications. Dried

fiber samples were cut into small pieces. Ten mg of fibers were placed in 5 mL Reacti-Vials™. Non-cellulosic matter in fibers was hydrolyzed with acetic-nitric acid reagent (73% acetic acid, 9% nitric acid and 18% water). The remaining cellulose was hydrolyzed with 67% sulfuric acid (v/v) and measured by a colorimetric assay with anthrone. Avicel PH-101 (FMC, Rockland, ME) was used as a cellulose standard. After cooling the solution on ice, it was transferred to a well in a 96-well microtiter plate. A plate reader (ThermoMax, Molecular Devices, Sunnyvale, CA) was used to measure A_{650} from the samples and standards. The average cellulose content for fibers was obtained from two biological and six technical replications.

Image analysis microscopy (IAM) of cross-sectioned fibers

Fully-developed fibers were harvested at 48 DPA when they were completely dried after the bolls were open at 42–44 DPA. The developed fibers were embedded, thin-section cut, and photographed using the method previously described (Boylston et al. 1993). The cross-sections were analyzed using image analysis software designed for measuring cross-sectional areas, perimeters and calculating circularity (Xu and Huang 2004). Average wall area (A) excluding lumen and perimeter (P) of the fiber cross sections were calculated from three hundred samples for each fiber cross-section. Circularity (θ) representing the degree of fiber cell wall development was calculated using the equation, $\theta = 4\pi A/P^2$ and the maturity ratio (MR) was converted from circularity by the equation, MR = θ/0.577 (Thibodeaux and Evans 1986; Wakelyn et al. 2010).

Polarized microscopy

Developing fibers (24, 28, 33, and 37 DPA) and developed fibers (48 DPA) were analyzed under polarized light to test for their relative maturity according to the general guidance of procedure 2 in ASTM D1442-06 (ASTM standard D1442-00 2012a). Images were taken by a Zeiss Axioplan universal microscope equipped with a Zeiss Axio Cam MRc5 (Carl Zeiss Microscopy, LLC, Thornwood, NY). Small arrays of developing and developed fibers were

gently combed to align the fibers and then mounted on a slide. The operator arranged the fibers to obtain a single layer of fiber on the slide.

Cottonscope measurement

Fiber maturity ratio (MR), fineness, and ribbon width were measured on the Cottonscope (Cottonscope Pty Ltd, Perth, Australia), using version 1.54 software. Internal polarized light microscopy was used to measure maturity, and the total length and width of a specified number of a minimum of 20,000 fiber snippets (approximately 1 mm cut fiber increments) were used to measure fineness and ribbon width. The Cottonscope has two maturity parameters—MR and MRBF. MRBF is the maturity due to the fiber's birefringence, as measured by polarized light microscopy (no normalization); MR is a normalized parameter in which the MRBF is normalized by the fiber's ribbon width (Rodgers et al. 2015). Six replicates were measured for each Cottonscope sample, composed of three sub-samples/loadings each measured in duplicate. For each sub-sample/loading, approximately 50.0 ± 0.3 mg of samples were produced by cutting fibers with a knife-blade cutter and weighed. The weighed fiber snippets were placed into the Cottonscope water bowl; fibers were individualized in water by agitating the snippets and measured as they passed under a color digital camera; a total of approximately 20,000 fiber snippets were measured in each run.

FT-Raman and ATR-FTIR spectroscopy

Cotton fiber bundles were stretched and pressed between metal plates to flatten the samples before analysis. Fibers were analyzed with a Nicolet 8700 FT-Raman spectrometer (Thermo Scientific, Waltham, MA). A diode-pumped Nd:YAG laser (1064 nm) was used as an excitation source and the Raman signal was collected with a liquid nitrogen cooled germanium detector. Spectra were taken in the region 250–3800 cm^{-1} at 8 cm^{-1} per step with averaging over 1000 scans. The beam power was set to 0.5–2.0 W. To prevent sample burning, the beam spot was translated to different locations on the sample during data acquisition using a camera and motorized stage (μView, DXR). Spectra were baseline corrected and normalized with the peak intensity at 1098 cm^{-1}.

ATR-FTIR spectra were collected using a Nicolet 8700 spectrometer (Thermo Scientific, Waltham, MA) equipped with a smartiTR diamond ATR unit and a deuterated triglycine sulfate detector. For the IR measurement, a large number of cotton fibers were twisted in to a single thick bundle which covered the entire sampling area (1.5 mm diameter) of the ATR window cell. Three spectra were taken in the region 650–3800 cm^{-1} at 2 cm^{-1} per step with averaging over 100 scans from each biological sample at various DPA. Average results of two independent biological samples were used for principal component analysis (PCA). Each spectrum was baseline corrected and then normalized at 1030 cm^{-1} peak intensity subjectively according to the method that was previously described (Lee et al. 2015a, b).

Sum frequency generation (SFG) vibrational spectroscopy

The details of SFG measurements were published previously (Barnette et al. 2011). The SFG spectrometer (EKSPLA) was pumped by a Nd:YAG laser, 1064 nm at 10 Hz (pulse duration = 27 ps). An optical parameter generator/amplifier (OPG/OPA) was pumped with 532 and 1064 nm and tuned to 2.3–10 μm with <6 cm^{-1} bandwidth. All spectra were collected using *ssp* polarization combination: SFG signal = s-polarized, visible = s-polarized and IR = p-polarized. The incidence angles for visible and IR pulses were 60° and 56° from the surface normal and were overlapped spatially and temporally on each sample. The SFG signal was collected using a beam collimator to enhance the collection efficiency of the scattered SFG photons near the phase matching angle in reflection geometry. The SFG signal was filtered through a monochromator and detected with a photomultiplier tube. The SFG intensity was normalized with incident IR and visible laser intensities. SFG spectra were taken at 4 cm^{-1}/step in the CH stretching region (2700–3050 cm^{-1}) and 8 cm^{-1}/step in the OH stretching region (3096–3800 cm^{-1}). The lower frequency region (1000–1400 cm^{-1}) is challenging to interpret because the skeletal stretching modes are highly delocalized (Lee et al. 2013); thus, this region was not analyzed in this study. The probe volume was estimated to be $\sim 150 \times 200$ μm^2 wide and ~ 20 μm deep from the external surface, governed by the IR beam attenuation in the sample (Kafle et al. 2014). The

protocol for SFG spectra acquired from cotton fibers is identical to our previous study (Lee et al. 2015b). Briefly, the air dried fibers were tightly twisted into ~ 2 mm diameter bundles, fixed on a glass slides and pressed firmly between metal plates to minimize the effects of sample roughness on SFG signal intensity. For each DPA the intensities of the 2944 and 3320 cm^{-1} peaks were analyzed at 15 locations per sample and were averaged to create the representative spectrum for each DPA. The CH_2 and OH areas were calculated by peak deconvolution (Lee et al. 2014) using OriginPro8 (OriginLab, Northampton, MA).

X-ray diffraction (XRD)

XRD experiments were performed with a PANalytical Empyrean diffractometer (PANalytical, Netherlands) equipped with a Cu X-ray source ($\lambda = 1.5404$ Å) operated at 45 kV and 40 mA, and the instrumental profile was calibrated with LaB_6 (NIST 660a). Fully dried cotton samples were ground in a Wiley mill to 20 mesh and hand pressed into pellets. Scans were acquired in the 2θ range of 8°–45° at 0.05° step. All XRD experiments were run in duplicate. The procedures using a peak deconvolution method for cellulose crystallinity and crystal width were previously described (Lee et al. 2015b). The cellulose crystallinity values calculated from the XRD data are method-dependent and the results are taken as a qualitative index to compare the trends within the cotton fiber samples harvested at different DPA (Lee et al. 2015a). The Scherrer formula, $D_{200} = K \cdot \lambda / \beta \cdot \cos\theta$ was used to calculate the crystal width across the (200) plane. D_{200} is the crystal size perpendicular to the (200) plane, K is the Scherrer constant (=0.9) (Kim et al. 2013c), λ is the wavelength of the X-ray source, θ is the Bragg angle and β is the full width at half maximum (FWHM) of the (200) peak. The diffraction data were also analyzed by the Rietveld method that is incorporated in the MAUD software (Lutterotti 2010). Rietveld refinements are undertaken by introducing small groups of variables in steps, taking care of the most important ones first. In the present studies, the overall scale factor to relate the observed and calculated intensity (1 parameter), a linear background (2 parameters), and the unit cell a-axis were refined initially. The following step added a quadratic parameter for the background (1 parameter), the monoclinic angle γ (1 parameter) and the

isotropic crystallite size (1 parameter). The third step added refinement of the March–Dollase parameter for preferred orientation (except where noted, 1 parameter), and the final step introduced a second phase to represent amorphous material (2 parameters).

Principal component analysis (PCA)

IR and Raman spectra for all samples were baseline corrected and normalized prior to a PCA algorithm to find the unbiased characteristics of TM-1 and *im* cotton fibers at different developmental stages. Separate PCA calculations were performed for respective IR and Raman spectra using a chemometric software (Unscrambler8.0, CAMO, Woodbridge, NJ).

Results and discussion

Comparison of HVI and AFIS fiber properties for *im* and TM-1

Fiber properties measured by HVI showed a significant difference in the MIC values from fully developed fibers between the *im* and TM-1 (Table 1). The MIC value of the *im* fibers (3.17) was only 76% (p value < 0.0001) as large as that of TM-1 fibers (4.18). The MIC value represents a combination of the maturity (degree of cell wall thickening) and fineness (mass per unit length) of cotton fibers. Therefore, the *im* fibers were either thinner or finer (or thinner and finer) than the TM-1 fibers. There were few but noticeable differences of the fiber UHML lengths between the NILs. The *im* fibers (31.3 mm) were slightly shorter (97%) than the TM-1 fibers

(32.3 mm). The strength of the *im* fibers (30.68 g/tex) was also significantly lower (88%, p value = 0.001) than that of TM-1 fibers (35.02 g/tex). Uniformity and elongation values did not show any significant difference between the NILs.

Most upland cotton varieties grown in regular US cotton fields reach their full maturity at 40–50 DPA (Haigler et al. 2012; Kim 2015; Snider and Oosterhuis 2015). Fiber development is greatly affected by environmental factors in addition to genetic factors (Bradow and Davidonis 2000). Thus, fiber development under abiotic stress from cold temperature or drought is often delayed. There are a few reports showing that upland cotton varieties grown in pots reached full maturity at approximately 60 DPA (Abidi et al. 2008, 2010; Lee et al. 2015b).

The HVI results showed that the bundle strength of the *im* fiber was weaker than the TM-1 fiber. The HVI determines bundle fiber strength (g/tex) by normalizing the breaking force (g) with the fineness value (tex). Thus, the bundle fiber strength of the *im* fiber can be reduced because of decreased breaking force or increased fineness value.

Fiber maturity ratio (MR) was measured by the AFIS instrument that is used to predict spinning performance and yarn quality since the 1980s (Shofner et al. 1988). Although there were significant differences of the MIC values between the NILs (Table 1), multiple AFIS measurements failed to detect significant differences of MR values between the NILs (Supplementary information Table S1). These results were consistent with the previous reports showing that AFIS measurements detected little MR differences between the NILs whereas HVI and IAM measurements monitored significant MR differences between

Table 1 HVI physical properties of fully developed (48 DPA) *im* and TM-1 wild type fibers

Physical properties	*im*			TM-1			Ratio (*im*/TM-1)	p value by t test[b]
	Mean	SD	Rep.	Mean	SD	Rep.		
Micronaire (MIC)	3.2	0.1	5	4.2	0.3	5	0.76	<0.0001***
UHML[a] (mm)	31.29	0.08	5	32.24	0.08	5	0.97	<0.0001***
Uniformity (%)	85.42	0.63	5	86.16	0.95	5	0.99	0.185
Strength (g/tex)	30.68	1.11	5	35.02	1.59	5	0.88	0.001**
Elongation (%)	4.54	0.30	5	4.84	0.29	5	0.94	0.147

[a] Upper-half mean fiber length

[b] Statistical significance was shown at the probability levels under * 0.05, ** 0.01, and *** 0.001

them (Kim et al. 2013a; Kothari et al. 2007). Therefore, we further analyzed the NILs using Cottonscope and IAM methods.

Qualitative comparisons of fiber morphologies between *im* and TM-1

Polarized optical microscopy was used to qualitatively compare convolutions and birefringence intensity at various developmental time points (Fig. 2). Developing fibers at the SCW thickening stage (24, 28, 33, and 37 DPA) and fully developed fibers at 48 DPA were dried and compared between the NIL fibers. At 24 and 28 DPA, most developing fibers of both NILs were blue color with few convolutions. At 33 DPA, yellow color and convolutions appeared. The yellow color intensity represents birefringence that was generated from organized crystalline material. The development of birefringence indicates the synthesis and deposition of the crystalline arrays of CMFs in the SCW of the cotton fibers (Seagull et al. 2000). More mature fibers appeared yellow, while less mature fibers appeared blue. The interference colors have been related to measures of relative fiber maturity (Schwarz and Hotte 1935). In both NIL fibers, higher birefringence intensity was commonly detected as fibers became thicker despite some levels of natural variation (Fig. 2). The similarities of polarized images (birefringence intensity and fiber convolution) between the NIL fibers do not support the previous hypothesis that the SCW cellulose

biosynthesis of the *im* fibers might be retarded (Benedict et al. 1994; Kohel and McMichael 1990; Kohel et al. 2002).

Quantitative comparisons of fiber wall thickness for *im* and TM-1 by IAM and Cottonscope

Despite the wide use of MIC and MR values from HVI and AFIS as a means for determining the quality of fibers, yarns and textiles, they are not designed for biological studies and do not necessarily represent the actual degree of cotton fiber wall thickness (Thibodeaux and Evans 1986; Thibodeaux and Rajasekaran 1999). Thus, the wall thicknesses of fully developed TM-1 and *im* fibers at 48 DPA were quantitatively and directly measured by the IAM method (Thibodeaux and Evans 1986; Wakelyn et al. 2010). The images of cross-sectioned NILs showed that the SCWs of the developed *im* fibers were visibly thinner than the developed TM-1 fibers (Fig. 3a). The circularity (θ) representing the degree of fiber cell wall thickness was calculated from the cell wall area and perimeter that were directly measured from three hundred cross-sections of dried fibers at 48 DPA and was converted to the MR value. The MR value of the developed *im* fibers at 48 DPA (0.71) was significantly lower (67%) than that of the developed TM-1 fibers at 48 DPA (1.06). Despite the large variation of standard errors of TM-1 (0.21) and *im* (0.19), there were statistically significant differences (p value < 0.0001) detected for the developed NIL fibers.
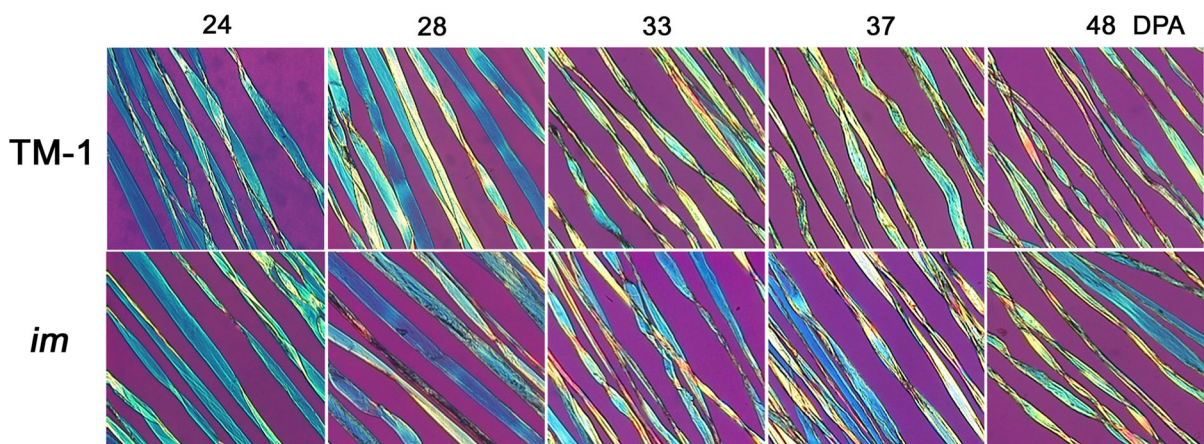
Fig. 2 Comparisons of polarized microscopic images of TM-1 and *im* fibers. Developing fibers (24, 28, 33, and 37 DPA) and fully developed fibers (48 DPA) of the NILs were photographed by polarized microscopy. Less mature fibers appeared *blue color*, whereas more mature fibers appeared *yellow color* that represents birefringence generated from organized crystalline cellulose. (Color figure online)

(a)

(b)
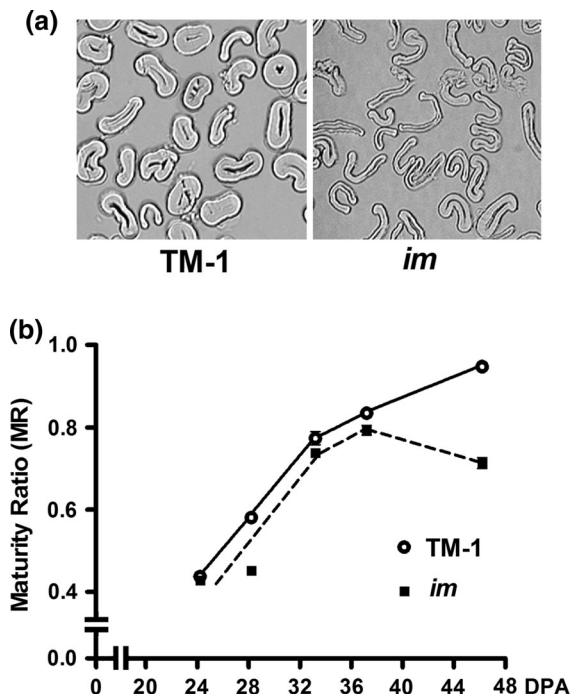
Fig. 3 Comparisons of fiber cell wall thickness between TM-1 and *im* fibers at various developmental stages. **a** Cross-sectioned Images of fully developed NIL fibers at 48 DPA. **b** Fiber maturity ratio (MR) values of developing fibers (24, 28, 33, and 37 DPA) and developed fibers (48 DPA) were compared according to the values measured from dried fibers at various DPA by Cottonscope. *Error bars* represent standard errors of the mean

We also measured fiber maturity of the NILs during fiber development using the Cottonscope (Fig. 3b). The average MR value of the *im* fibers at each time point was measured from dried fibers at five different time points (24, 28, 33, 37, and 48 DPA). The MR values of the *im* fibers between 24 and 48 DPA were significantly (p value < 0.0001) lower than those of the TM-1 fibers at the same developmental period (Fig. 3b). During the SCW cellulose biosynthesis stage from 24 to 37 DPA, the MR values of developing *im* fibers increased from 0.428 to 0.793 as those of developing TM-1 fibers increased from 0.437 to 0.835.

When the NIL fibers were fully developed at 48 DPA, the MR values measured by Cottonscope for the TM-1 fibers (0.948) continuously increased from 37 DPA (0.835). In contrast, the MR values of the *im* fibers did not increase from 37 DPA (0.793) to 48 DPA (0.713). These results suggest that late SCW and/ or maturation stages (37–48 DPA) might be involved in increasing fiber maturity in TM-1 fibers, but not in *im*

fibers. The Cottonscope originally measures the degree of birefringence intensity and converts its values to MR values using calibrations versus standard MR values measured from Upland cotton (Brims and Hwang 2010; Kim et al. 2014). The birefringence is generated from the organized crystalline cellulose in cotton fibers (Seagull et al. 2000). Thus, the lower Cottonscope MR value of the *im* fibers at 48 DPA (Fig. 3) might imply less organization of the cellulose microfibrils in the *im* fibers at 48 DPA. Consistent with the lower birefringence intensity detected from the *im* fibers by Cottonscope (Fig. 3b), less organized CMF packing was later detected in the *im* fibers by SFG spectroscopy (Fig. 8).

Consistent with the significant differences of the MIC values between the TM-1 and *im* fibers (Table 1), the Cottonscope and IAM results clearly showed the significant MR differences between the NILs (Fig. 3a, b). However, AFIS measurements showed little if any detectable difference between the MR values of the TM-1 and *im* fibers (Supplementary information Table S1). These results were similar to the previous reports (Kim et al. 2013a; Kothari et al. 2007). Therefore, we are investigating whether misclassification of the AFIS MR values from the *im* fibers was caused by the unique nature of the *im* fibers or by the insufficient sensitivity of the AFIS instrument that has been recently reported (Kim et al. 2014; Paudel et al. 2013; Rodgers et al. 2013).

Quantitative comparisons of fiber fineness and ribbon width for *im* and TM-1

Fiber fineness was measured in terms of ribbon width or linear density (mtex) from developing and developed NIL fibers. First, Cottonscope analysis was used to measure average ribbon widths of the NILs (Fig. 4a). Average ribbon widths of TM-1 fibers significantly decreased (p value $= 0.003$) from 24 (17.83 μm) to 48 DPA (15.42 μm). The same significantly decreasing pattern (p value $= 0.008$) was also found in the *im* from 24 (17.63 μm) to 48 DPA (16.01 μm). However, there was no significant (p value $= 0.525$) difference of the ribbon width between the NILs at the corresponding time points.

The linear density values were directly determined by a gravimetric fineness method that is considered to be a reference method (Montalvo 2005). Average linear density values of the TM-1 fibers significantly
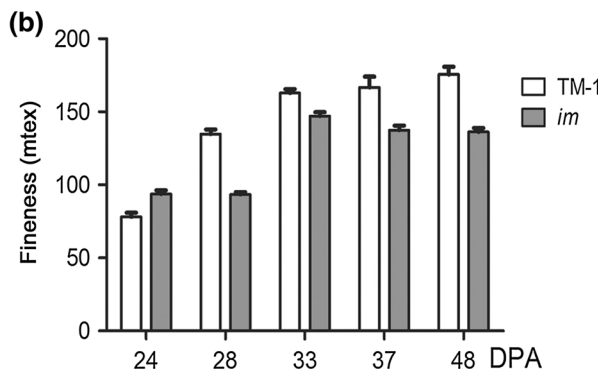
(a)

(b)
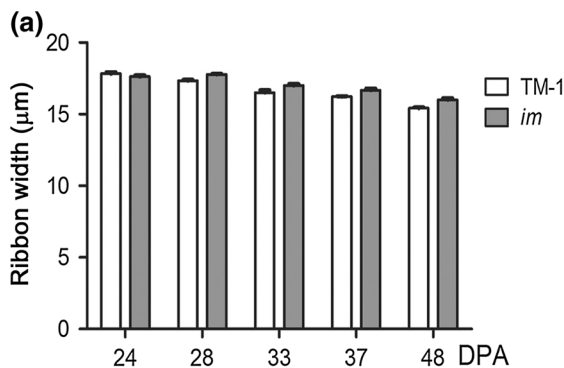
Fig. 4 Comparions of ribbon width and fineness of developing fibers between NILs. Developing fibers (24–37 DPA) and developed fibers (48 DPA) were measured to determine fiber ribbon width by Cottonscope (**a**) and fiber fineness by gravimetric fineness method (**b**). Fineness values are smaller for finer fibers

increased (p value < 0.0001) from 24 (78.15 mtex) to 48 DPA (175.56 mtex) as the same increasing pattern (p value < 0.0001) in the *im* fibers from 24 (93.70 mtex) to 48 DPA (136.30 mtex) (Fig. 4b). The linear density values of the *im* fibers (28–48 DPA) were significantly (p value < 0.0001) lower than those of the TM-1 fibers.

Consistent with the lower gravimetric fineness ratio (77%) of the developed *im* fibers (136.30 mtex) over the TM-1 fibers (175.56 mtex), the fineness values of the developed *im* fibers measured by the Cottonscope (75%) or IAM (62%) were significantly lower than those of the developed TM-1 fibers (Supplementary information Table S2). The results suggested that the amount of cellulose for the same length of the *im* fibers is lower than that of the TM-1 fibers, and the *im* fiber cell walls may be less dense than the TM-1 fiber cell walls. It also supported the finding that the AFIS instrument was insensitive to the differences of fineness between the NILs.

Comparisons of cellulose content (weight %) between NIL fibers

Cellulose contents between the NIL fibers at different developmental stages (10, 17, 24, 28, 33, 37, and 48 DPA) were compared. The average cellulose content showed similar increasing patterns during fiber development between TM-1 and *im* (Fig. 5). There were slight variations of cellulose content at some development time points like 17 and 28 DPA between TM-1 and *im*. The SCW cellulose production in the *im* fibers appeared to be slightly delayed between 17 and 28

Fig. 5 Comparisons of cellulose contents between TM-1 wild type and *im*. Cellulose contents of two NIL fibers were compared at different days post anthesis (DPA) covering entire fiber development

DPA, but there were few detectable differences from 33 to 48 DPA. Fully developed fibers (48 DPA) showed almost identical cellulose content between TM-1 (90.1 ± 1.4%) and *im* (93.9 ± 6.1%). During the entire fiber development between the NILs, there was no significant difference (p value = 0.288) on the cellulose content pattern. Thus, we concluded that the NILs shared a common developmental stage for SCW cellulose biosynthesis and similar cellulose contents (based on weight %) although the cellulose mass per unit length was different as described in Fig. 4b. Our results disagreed with the previous reports of significantly lower cellulose content in the *im* fibers as compared with the TM-1 fibers (Benedict et al. 1994; Wang et al. 2014). Therefore, we further tested the NIL fibers with two addition assays including ATR-FTIR and Raman spectroscopy to confirm our finding of the common developmental stages of the NILs.

ATR-FTIR analysis of NIL fibers

The cellulose and matrix polymer composition during the fiber development was monitored using ATR-FTIR and PCA (Lee et al. 2015b). Figure 6a, b show the ATR-FTIR spectra for TM-1 and *im* cotton fibers at 10–48 DPA, respectively. The first principal component (PC1) shown in Fig. 6c describes 93% of the variances in the TM-1 and *im* spectra. The negative peaks in the PC1 loading plot (Fig. 6c) included: water peaks (H–O–H bending peak at ~1640 cm^{-1} and broad O–H stretch peak at 3100–3600 cm^{-1}), protein peaks (amide-I and amide-II bands at 1520–1650 cm^{-1}) and pectin peaks (C=O stretching vibration at 1740 cm^{-1}) (Abidi et al. 2014). In contrast, the peaks attributable to cellulose in the 890–1450 and 3270–3330 cm^{-1} are positive in the PC1 spectrum (Fig. 6c). The long-chain alkyl hydrocarbon peaks from cuticles (CH$_2$ stretch peaks at 2850 and 2926 cm^{-1}) were negative in *im* fibers, but positive in TM-1 fibers (Fig. 6c).

In the score plot shown in Fig. 6d, large negative scores of PC1 for 10 DPA cotton fibers are due to signals from non-cellulosic components (water, proteins, pectins and hydrocarbon in the cuticle). As the SCW cellulose was produced at the transition from 10 to 17 DPA, the PC1 scores significantly increased. During the fiber wall thickening stage (17–37 DPA), the cotton fibers are composed of SCW cellulose, which led to a significant increase in PC1 scores. Previously, the progression of PC1 scores with DPA was indicative of the transition from PCW to SCW in the cotton fiber (Lee et al. 2015b). Thus, the PC1 scores of the ATR-FTIR spectra were a good indicator
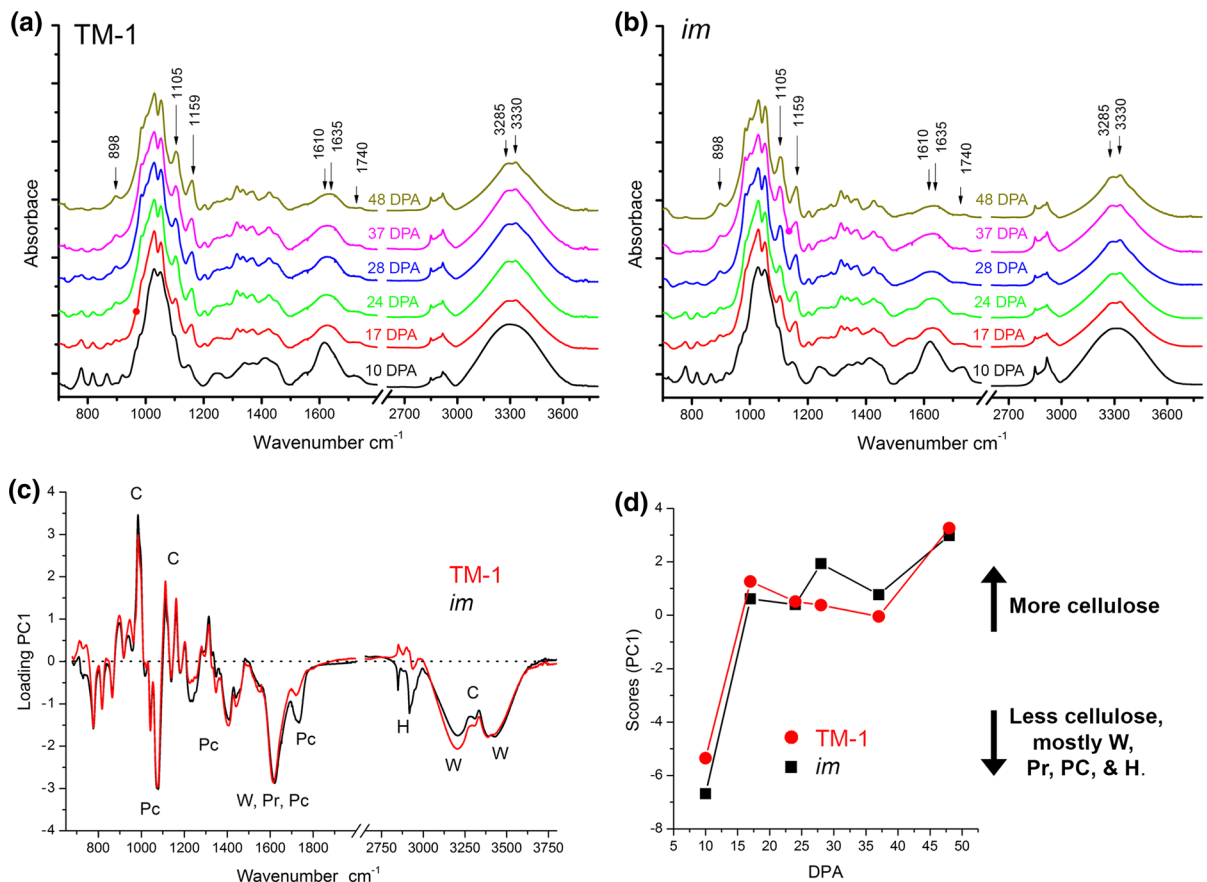
Fig. 6 ATR-IR spectra of cotton fiber bundles at 10 to 48 DPA for **a** TM-1 and **b** *im* mutant. PCA of entire data set and **c** loading plot of principal component 1, PC-1 (93% explained variance) representing the predominant spectral elements. The letters W,
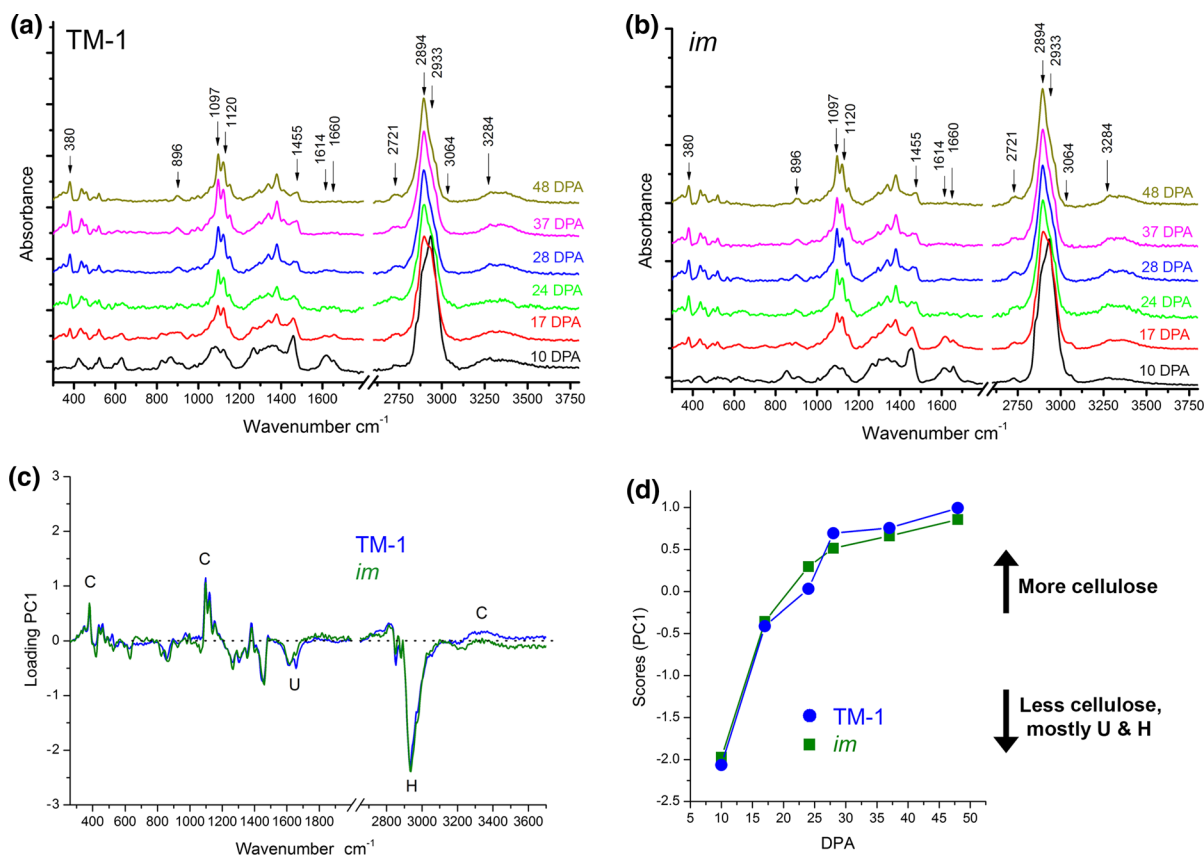
C, Pr, Pc, and H indicate water, cellulose, protein, pectin, and hydrocarbon components, respectively. The *dotted line* represents zero PC1 loading. **d** Plot of PC1 score versus DPA

to distinguish 10 DPA as the stage of PCW synthesis which quickly transitioned to SCW synthesis at 17 DPA in both TM-1 and *im*. Consistent with the trend of cellulose content observed for the NILs (Fig. 5), the FTIR spectroscopy also showed the common fiber developmental stages and similar cellulose and matrix polymer compositions during the NIL fiber development (Fig. 6d).

Raman spectroscopic analysis of NIL fibers

The Raman spectra of TM-1 and *im* fibers collected at 10–48 DPA are shown in Fig. 7a, b, respectively. The loading plot of the first principal component (PC1, 88% explained variance) in Fig. 7c showed positive peaks at locations that could be attributed to crystalline cellulose: 380, 1000–1150, 1300–1500, 2894 and 3357 cm^{-1}. The PC1 had negative peaks at 2883

and 2933 cm^{-1} (long-chain alkyl components of the cuticle and pectin) as well as 1614 and 1660 cm^{-1} (unsaturated hydrocarbon components) (Greene and Bain 2005). The PC1 score was negative for the 10 DPA cotton fibers and gradually increased during maturity (Fig. 7d). Similar to ATR-FTIR (Fig. 6d), the Raman PC1 scores indicated that 10 DPA cotton fibers were mostly PCW and 17–48 DPA cotton fibers were SCW cellulose. In the Raman spectrum of cellulose, the characteristic peak attributed to the crystalline phase occurs at 380 cm^{-1} (Agarwal et al. 2010). This peak became prominent in cotton fibers at 17 DPA (Fig. 7a, b). These results were consistent with the steady increase in cellulose content in the cotton fibers with development (Fig. 5). There were no differences between the Raman spectra (Fig. 7c) or PC1 scores (Fig. 7d) of TM-1 and *im* at the same DPA. Consistent with the results from cellulose content

Fig. 7 Raman spectra of cotton fiber bundles at 10 to 48 DPA for **a** TM-1 wild type and **b** *im*. PCA of entire data set and **c** loading plot of principal component 1, PC-1 (88% explained variance) representing the predominant spectral elements. The

letters *C*, *U*, *H* indicate cellulose, unsaturated hydrocarbon, and long-chain alkyl groups, respectively. The *dotted line* represents zero PC1 loading. **d** Plot of PC1 score versus DPA

(Fig. 5) and ATR-FTIR (Fig. 6d), the Raman spectroscopy results also showed that the developmental changes in chemical compositions were similar for both the NILs (Fig. 7d).

SFG analysis of cellulose from the NIL fibers

SFG has recently been applied to study cellulose structure in cotton fibers (Hieu et al. 2011; Kafle et al. 2014; Lee et al. 2015b). SFG is a non-linear optical spectroscopy where the signal intensity is proportional to the non-centrosymmetrically arranged vibration modes over the mesoscale length (estimated to be around 300 nm) which is defined by the SFG coherence length (Lee et al. 2014, 2015b). At the mesoscale, the non-cellulosic polymers in plant cell walls (e.g. hemicellulose and lignin) are amorphous and are SFG-inactive (Barnette et al. 2011; Park et al. 2013). In contrast, the cellulose crystals are inherently noncentrosymmetric. This allows SFG to selectively probe the vibration modes from the crystalline cellulose in the cotton fibers without contributions from amorphous matrix polymers or amorphous phase of cellulose (Barnette et al. 2011). Additionally, the mesoscale spatial packing of cellulose crystallites influences the SFG intensity ratio of the peaks corresponding to alkyl (CH and CH_2) and hydroxyl (OH) stretching vibrations (Lee et al. 2014, 2015b). Therefore, the absolute SFG intensity can be related to the cellulose mass fraction only when the spatial packing in the sample does not change. The absolute SFG intensity and CH_2/

OH intensity ratio could reveal structural development of CMFs at various stages.

The SFG spectra of TM-1 and *im* fibers from 10 to 48 DPA are shown in Fig. 8. At 10 DPA there were no SFG signals detected for either TM-1 or *im* fibers in our experimental condition suggesting that during PCW synthesis the CMFs are sparsely packed at the mesoscale (Fig. 8a, b). It has been shown that CMFs with insufficient mesoscale ordering do not produce SFG signals despite the cotton fibers having a 10% wt. cellulose content (Fig. 5) which is above the detection threshold of SFG (Lee et al. 2015b). Additionally, the absence of the 380 cm^{-1} peak in Raman spectra of 10 DPA (Fig. 7a, b) also suggests that cellulose crystallinity is very low. The discernible crystalline cellulose SFG signals at 2944 and 3320 cm^{-1} appeared at 17 DPA. These are two characteristic peaks of cellulose in the SCWs of cotton, ramie and flax (Lee et al. 2014, 2015b).

To explore changes in mesoscale packing with development stage, the peak areas calculated from the Lorentzian peak fitting for the alkyl stretching region (2700–3000 cm^{-1}) and the hydroxyl stretching region (3100–3400 cm^{-1}) are plotted as a function of DPA in Fig. 8c. In the case of TM-1, the CH_2 SFG peak of cellulose increased steadily during the transition (17–28 DPA), late thickening (33–37 DPA) and maturation (37–48 DPA) stages; however, in the case of *im*, it increased only during the transition and late thickening stages and then slightly dropped during the maturation state. It was also noted that the OH SFG
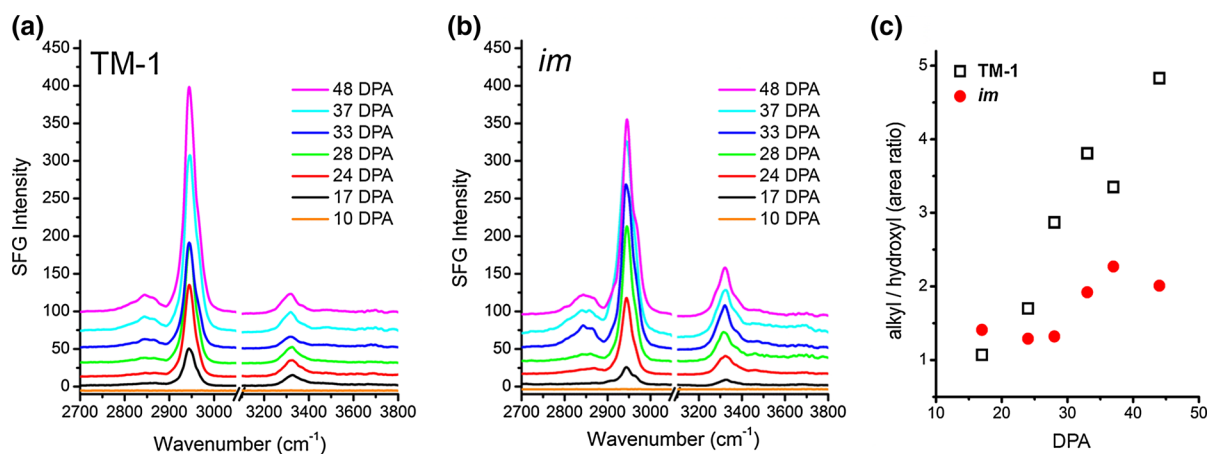
Fig. 8 SFG spectra during cotton fiber development for *G. hirsutum* cotton fibers from 10 to 48 DPA for **a** TM-1 wild type and **b** *im*. The y-axis scale is offset for each spectrum to allow intensities to be compared between spectra. **c** Alkyl/hydroxyl ratio SFG area ratio for TM-1 (*black square*) and *im* (*red circle*). (Color figure online)

peak of TM-1 did not grow significantly after 17 DPA, while that of *im* steadily increased further. Consequently, the alkyl/hydroxyl area ratio increased continuously from ~1 at 17 DPA to ~5 at 48 DPA for TM-1, while it leveled off at ~2 after 30 DPA in the case of *im* (Fig. 8c).

In previous SFG studies on *G. hirsutum* and *G. barbadense* cotton fibers, the changes in alkyl/hydroxyl ratio could be related to the mesoscale arrangement of CMFs (Lee et al. 2014, 2015b). If CMFs are laterally packed with adjacent microfibrils without specific control in their directionality, then the numbers of CMFs running in opposite directions would be similar. In that case, the opposite directionality or "antiparallel packing" of CMFs would result in the cancellation of the OH dipoles between adjacent microfibrils placed within the SFG coherence length. This cancellation would vary with the spacing between adjacent microfibrils (Lee et al. 2014). Although the molecular details are not fully understood yet, the cancellation effect due to the antiparallel packing of crystalline domains has been experimentally proven to be larger for the OH stretch dipoles than the CH_2 stretch dipoles (Lee et al. 2014). Based on this empirical observation, the high alkyl/hydroxyl area ratio can be interpreted as a better lateral packing of crystalline domains with overall antiparallel directionality in the mesoscale. Thus, the data shown in Fig. 8 suggest that the degree of lateral packing of CMFs keeps increasing in the cas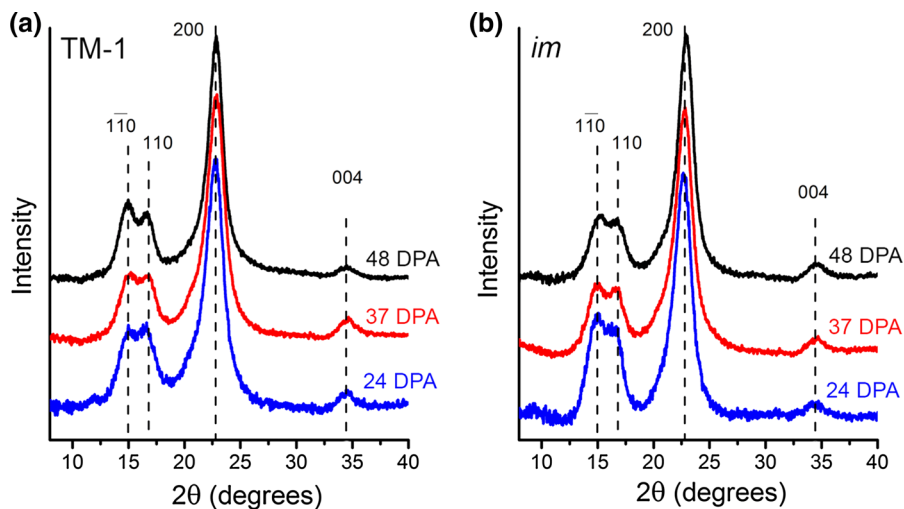e of TM-1 cotton fibers until the boll opens, whereas it does not increase after the SCW thickening state in the case of *im* fibers.

X-ray diffraction analysis of intact cotton fibers

Changes in crystallinity and crystal width during fiber development were investigated with XRD analysis. All tested TM-1 and *im* fibers showed the characteristic diffraction peaks for crystalline cellulose: $2\theta = 14.6°$, $16.4°$ and $22.7°$ corresponding to the $(1\bar{1}0)$, (110) and (200) reflections, respectively (Fig. 9a, b). The XRD results analyzed by the peak deconvolution method and Scherrer equation showed no significant difference between TM-1 wild type and *im* fibers in terms of crystallinity index (CI%) or crystal width of the (200) reflection (Table 2). It should be noted that the CI% calculation based on the deconvolution method is subject to the base line corrections as well as the sample mounting to XRD (Lee et al. 2015a). Also, the XRD peaks vary in a complex manner with the crystalline component concentration and crystallite size. Thus, the simple ratio of specific crystalline peak intensities or areas over the total intensity cannot be considered as true "crystallinity" (Lee et al. 2015a).

For that reason, the diffraction data were further analyzed by the Rietveld method that is incorporated in the MAUD software (Lutterotti 2010). The MAUD Rietveld program permits the intensities calculated from the background and the crystalline and amorphous phases. Figure 10 is a plot of these data,

Fig. 9 X-ray diffractograms of *G. hirsutum* cotton fiber bundles at 24, 37, and 48 DPA for **a** TM-1 and **b** *im*. Linear backgrounds were subtracted from raw data

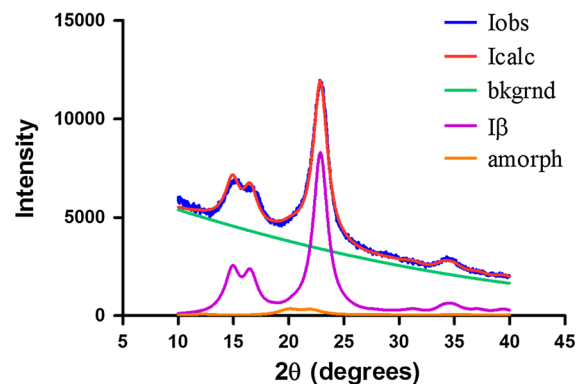**Table 2** XRD results obtained from TM-1 wild type and *im* fibers

[a] Calculated from the 200 peak width using the Scherrer equation

[b] Calculated from the peak deconvolution method

[c] Determined by the Rietveld method

Cotton lines	Properties	24 DPA	37 DPA	48 DPA
TM-1	Crystal size[a]	4.8 nm	4.6 nm	5.2 nm
	Crystallinity[b]	66%	68%	64%
	Crystalline cellulose Iβ content[c]	67.2%	85.1%	86.8%
	Amorphous cellulose content[c]	32.8%	14.9%	13.2%
im	Crystal size[a]	4.7 nm	4.8 nm	5.0 nm
	Crystallinity[b]	80%	66%	74%
	Crystalline cellulose Iβ phase[c]	98.8%	78.2%	86.8%
	Amorphous cellulose content[c]	1.2%	21. 8%	13.2%

depicting the analysis of TM-1 fibers at 48 DPA. Here, the observed data (Iobs) are different from those in Fig. 9a because the background has not been subtracted. In the analysis, the cellulose Iβ crystal structure (Nishiyama et al. 2002) was used as a model for the crystalline cellulose I phase, and the cellulose II crystal structure (Langan et al. 2001) was used for the amorphous phase based on the calculated diffraction pattern of the cellulose II with a 9° peak width at half height (Nam et al. 2016). A slightly curved line (bkgrnd) corresponds to the refined background, and the area under it (the sums of the intensity values at all 2θ points) contributes to the total calculated intensity (Icalc). The contribution for the amorphous scattering

Fig. 10 MAUD refinement of TM-1 fibers at 48 DPA, showing the individual contributions to the total calculated intensity and its comparison to the observed data. During refinement, the small introduced crystallite size of the cellulose II component (simulating amorphous cellulose) increased to give sharp enough peaks that it would be considered crystalline. The very small amount of indicated cellulose II is probably an artifact of the refinement. Iobs, observed experimental intensity; Icalc, calculated intensity; bkgrnd, refined background; Iβ, calculated cellulose Iβ intensity; amorph, amorphous cellulose intensity

(amorph) suggests that there is a small amount (1.3% of the total calculated) of cellulose II present. As indicated in Table S3, several samples had cellulose II crystals greater than 2 nm, but all had minimal amounts based on the integrated area. The crystallite size in MAUD is roughly 25% larger than the size calculated with the Scherrer equation (Luca Lutterotti, personal communication). We also note that the Rietveld crystallite sizes were uniformly larger when some added phase material was present in the MAUD analyses. At this time we do not understand the determination of the phase amounts in MAUD; they are clearly different than our simple calculations based on integration of the calculated intensities.

Despite the discrepancies, however, both the deconvolution and Rietveld analyses indicate that there is little difference among the diffraction patterns for the six samples considered herein. The results showed that the crystalline cellulose I phase and amorphous phase (86.8 and 13.2%, respectively, from the Rietveld analysis) of the developed TM-1 fibers at 48 DPA were little different from those (identical with ±0.1% error) of the developed *im* fibers at 48 DPA (Table 2). Based on the previous suggestion that crystalline cellulose biosynthesis might be retarded in the *im* fibers, higher amorphous cellulose and lower crystalline cellulose in the *im* fibers would be expected as compared to the wild type TM-1 fibers. However, our results suggested no significant difference between the developed TM-1 wild type and *im* fibers in terms of crystalline and amorphous cellulose contents (Supplementary information Tables 3S and 4S). In addition, the supplementary results suggested that the cellulose Iβ crystal structure (Nishiyama et al. 2002) provided a suitable model for the refinement of the fit of a cotton cellulose diffraction pattern (Supplementary information Table S3) and the

refined values of the unit cell a-axis and γ-angle were reasonably close to the determined values and consistent despite some variables (Supplementary information Table S4).

Conclusion

Using both traditional and innovative analytical techniques, we have characterized the physical and chemical properties of developing and developed fibers from the upland NIL cotton varieties, TM-1 and *im* that have been extensively studied for identifying potential molecular mechanisms regulating fiber wall thickness by genetic and genomic approaches. The *im* fibers were previously thought to suffer from retarded cellulose biosynthesis during fiber development. Our results from the Updegraff cellulose assay, Cottonscope, as well as FTIR, and Raman spectroscopy consistently showed common developmental stages and similar chemical compositions for the *im* and TM-1 fibers. XRD data also showed that both fibers have similar crystallinity. SFG analysis revealed that the thin cell wall of the *im* fiber is caused by disruption of mesoscale CMF organization or assembly in the cell wall, but not by the reduced cellulose content that was previously proposed (Benedict et al. 1994; Wang et al. 2014). The comprehensive phenotypic analyses of developing NIL fibers will be useful for bridging the gap between genotypic and phenotypic cotton researches, interpreting transcriptome profile data sets that have been dramatically expanded with recent cutting edged genomic techniques, and providing another way of dissecting functions of candidate genes involved in fiber wall thickness process.

References

Abidi N, Hequet E, Cabrales L, Gannaway J, Wilkins T, Wells LW (2008) Evaluating cell wall structure and composition of developing cotton fibers using Fourier transform infrared spectroscopy and thermogravimetric analysis. J Appl Polym Sci 107:476–486

Abidi N, Cabrales L, Hequet E (2010) Fourier transform infrared spectroscopic approach to the study of the secondary cell wall development in cotton fiber. Cellulose 17:309–320

Abidi N, Cabrales L, Haigler CH (2014) Changes in the cell wall and cellulose content of developing cotton fibers investigated by FTIR spectroscopy. Carbohyd Polym 100:9–16

Agarwal UP, Reiner RS, Ralph SA (2010) Cellulose I crystallinity determination using FT-Raman spectroscopy: univariate and multivariate methods. Cellulose 17:721–733

ASTM standard D1442-00 (2012a) Standard test method for maturity of cotton fibers (sodium hydroxide swelling and polarized light procedures). American Society for Testing and Materials, West Conshohocken

ASTM standard D1577-07 (2012b) Standard test method for linear density of textile fibers. Option A, Fiber bundle weighing. American Society for Testing and Materials, Philadelphia

Atalla RH, Vanderhart DL (1984) Native cellulose: a composite of two distinct crystalline forms. Science 223:283–285

Barnette AL et al (2011) Selective detection of crystalline cellulose in plant cell walls with sum-frequency-generation (SFG) vibration spectroscopy. Biomacromolecules 12:2434–2439

Benedict CR, Kohel RJ, Jividen GM (1994) A cellulose cotton fiber mutant: effect on fiber strength. In: Jividen GM, Benedict CR (eds) Proceedings of biochemistry of cotton workshop. Cotton Incorporated, Raleigh, pp 115–120

Benedict CR, Kohel JR, Lewis HL (1999) Cotton fiber quality. In: Smith CW, Cothren JT (eds) Cotton:origin, history, technology, and production. Wiley, New York, pp 269–288

Boylston EK, Thibodeaux DP, Evans JP (1993) Applying microscopy to the development of a reference method for cotton fiber maturity. Text Res J 63:80–87. doi:10.1177/004051759306300203

Bradow JM, Davidonis GH (2000) Quantitation of fiber quality and the cotton production-processing interface: a physiologist's perspective. J Cotton Sci 4:34–64

Brims M, Hwang H (2010) Introducing Cottonscope: a rapid and precise measurement of cotton fibre maturity based on siromat. National Cotton Council, New Orleans

Greene PR, Bain CD (2005) Total internal reflection Raman spectroscopy of barley leaf epicuticular waxes in vivo. Colloids Surf B 45:174–180

Haigler C (2010) Physiological and anatomical factors determining fiber structure and utility. In: Stewart JM, Oosterhuis DM, Heitholt JJ, Mauney JR (eds) Physiology of cotton. Springer, New York, pp 33–47

Haigler CH, Betancur L, Stiff MR, Tuttle JR (2012) Cotton fiber: a powerful single-cell model for cell wall and cellulose research. Front Plant Sci 3(104):1–7

Hieu HC, Tuan NA, Li H, Miyauchi Y, Mizutani G (2011) Sum frequency generation microscopy study of cellulose fibers. Appl Spectrosc 65:1254–1259

Kafle K, Xi X, Lee CM, Tittmann BR, Cosgrove DJ, Park YB, Kim SH (2014) Cellulose microfibril orientation in onion (*Allium cepa* L.) epidermis studied by atomic force microscopy (AFM) and vibrational sum frequency generation (SFG) spectroscopy. Cellulose 21:1075–1086

Kim HJ (2015) Fiber biology. In: Fang DD, Percy RG (eds) Cotton. Agronomy monograph, 2nd edn. American Society of Agronomy, Crop Science Society of America, and Soil Science Society of America, Madison, pp 97–127

Kim HJ, Triplett BA (2001) Cotton fiber growth in planta and in vitro. Models for plant cell elongation and cell wall biogenesis. Plant Physiol 127:1361–1366

Kim HJ, Moon HS, Delhom CD, Zeng L, Fang DD (2013a) Molecular markers associated with the immature fiber (im) gene affecting the degree of fiber cell wall thickening in cotton (*Gossypium hirsutum* L.). Theor Appl Genet 126:23–31

Kim HJ, Tang Y, Moon HS, Delhom CD, Fang DD (2013b) Functional analyses of cotton (*Gossypium hirsutum* L.) immature fiber (im) mutant infer that fiber cell wall development is associated with stress responses. BMC Genom 14:889

Kim SH, Lee CM, Kafle K (2013c) Characterization of crystalline cellulose in biomass: basic principles, applications, and limitations of XRD, NMR, IR, Raman, and SFG. Korean J Chem Eng 30:2127–2141

Kim HJ, Rodgers J, Delhom C, Cui X (2014) Comparisons of methods measuring fiber maturity and fineness of Upland cotton fibers containing different degree of fiber cell wall development. Text Res J 84:1622–1633

Kohel RJ, McMichael SC (1990) Immature fiber mutant of upland cotton. Crop Sci 30:419–421

Kohel R, Richmond T, Lewis C (1970) Texas marker-1. Description of a genetic standard for *Gossypium hirsutum* L. Crop Sci 10:670–671

Kohel RJ, Quisenberry JE, Benedict CR (1974) Fiber elongation and dry weight changes in mutant lines of cotton. Crop Sci 14:471–474

Kohel RJ, Stelly DM, Yu JZ (2002) Tests of six cotton (*Gossypium hirsutum* L.) mutants for association with aneuploids. J Hered 93:130–132

Kothari N, Abidi N, Hequet E (2007) Wilkins T Fiber quality variability within a plant. In: World cotton research conference-4, Lubbock, 10–14 Sept 2007. International Cotton Advisory Committee (ICAC)

Langan P, Nishiyama Y, Chanzy H (2001) X-ray structure of mercerized cellulose II at 1 Å resolution. Biomacromol 2:410–416

Lee CM, Mohamed NM, Watts HD, Kubicki JD, Kim SH (2013) Sum-frequency-generation vibration spectroscopy and density functional theory calculations with dispersion corrections (DFT-D2) for cellulose Iα and Iβ. J Phys Chem B 117:6681–6692

Lee CM, Kafle K, Park YB, Kim SH (2014) Probing crystal structure and mesoscale assembly of cellulose microfibrils in plant cell walls, tunicate tests, and bacterial films using vibrational Sum Frequency Generation (SFG) spectroscopy. Phys Chem Chem Phys 16:10844–10853

Lee CM, Dazen K, Kafle K, Moore A, Johnson DK, Park S, Kim SH (2015a) Correlations of apparent cellulose crystallinity determined by XRD, NMR, IR, Raman, and SFG methods. In: Rojas OJ (ed) Cellulose chemistry and properties: fibers, nanocelluloses and advanced materials. Advances in polymer science. Springer International Publishing, Switzerland, pp 115–131

Lee CM, Kafle K, Belias DW, Park YB, Glick RE, Haigler CH, Kim SH (2015b) Comprehensive analysis of cellulose content, crystallinity, and lateral packing in *Gossypium hirsutum* and Gossypium barbadense cotton fibers using sum frequency generation, infrared and Raman spectroscopy, and X-ray diffraction. Cellulose 22:971–989

Li F et al (2015) Genome sequence of cultivated Upland cotton (*Gossypium hirsutum* TM-1) provides insights into genome evolution. Nat Biotechnol 33:524–530

Lutterotti L (2010) Total pattern fitting for the combined size–strain–stress–texture determination in thin film diffraction. Nucl Instrum Methods Phys Res, Sect B 268:334–340

Moharir AV (1998) True-spiral angle in diploid and tetraploid native cotton fibers grown at different locations. J Appl Polym Sci 70:303–310

Moharir AV, Van Langenhove L, Van Nimmen E, Louwarie J, Kiekens P (1999) Stability of X-ray cellulose crystallite orientation parameters in native cotton with change of location and year of growth. J Appl Polym Sci 72:269–276

Montalvo JGJ (2005) Relationships between micronaire, fineness, and maturity. Part I. Fundamentals. J Cotton Sci 9:81–88

Nam S, French AD, Condon BD, Concha M (2016) Segal crystallinity index revisited by the simulation of X-ray diffraction patterns of cotton cellulose Iβ and cellulose II. Carbohyd Polym 135:1–9

Nishiyama Y, Langan P, Chanzy H (2002) Crystal structure and hydrogen-bonding system in cellulose Iβ from synchrotron X-ray and neutron fiber diffraction. J Am Chem Soc 124:9074–9082

Park YB, Lee CM, Koo B-W, Park S, Cosgrove DJ, Kim SH (2013) Monitoring meso-scale ordering of cellulose in intact plant cell walls using sum frequency generation spectroscopy. Plant Physiol 163:907–913

Paudel D, Hequet E, Noureddine A (2013) Evaluation of cotton fiber maturity measurements. Ind Crops Prod 45:435–441

Percy R, Hendon B, Auld D (2015) Qualitative genetics and utilization of mutants. In: Fang DD, Percy RG (eds) Cotton. Agronomy monograph, vol 57, 2nd edn. American Society of Agronomy, Crop Science Society of America, and Soil Science Society of Americ, Madison, pp 155–186

Rodgers J, Delhom C, Hinchliffe D, Kim HJ, Cui X (2013) A rapid measurement for cotton breeders of maturity and fineness from developing and mature fibers. Text Res J 83:1439–1451. doi:10.1177/0040517512471744

Rodgers J, Naylor GR, Cui X, Delhom C, Hinchliffe D (2015) Cottonscope fiber maturity, fineness, and ribbon width

measurements with different sample sizes. Text Res J 85:897–911

Schwarz E, Hotte G (1935) Micro-determination of cotton fibre maturity in polarized light. Text Res J 5:370–376

Seagull RW, Oliveri V, Murphy K, Binder A, Kothari S (2000) Cotton fiber growth and development 2. Changes in cell diameter and wall birefringence. J Cotton Sci 4:97–104

Shofner FM, Williams GF, Bragg KC, PE Sasser (1988) Advanced fiber information system: a new technology for evaluating cotton. Paper presented at the conference of the Textile Institute, Coventry, Dec 7–8, 1988

Snider JL, Oosterhuis DM (2015) Physiology. In: Fang DD, Percy RG (eds) Cotton. Agronomy monograph, vol 57, 2nd edn. American Society of Agronomy, Crop Science Society of America, and Soil Science Society of America, Madison, pp 339–400

Thibodeaux DP, Evans JP (1986) Cotton fiber maturity by image analysis. Text Res J 56:130–139

Thibodeaux DP, Rajasekaran K (1999) Development of new reference standards for cotton fiber maturity. J Cotton Sci 3:188–193

Thyssen GN et al (2016) The immature fiber mutant phenotype of cotton (*Gossypium hirsutum*) is linked to a 22-bp frame-shift deletion in a mitochondria targeted pentatricopeptide repeat gene. G3: Genes| Genomes| Genetics 6:1627–1633

Updegraff DM (1969) Semimicro determination of cellulose in biological materials. Anal Biochem 32:420–424

Wakelyn PJ et al (2010) Cotton fiber chemistry and technology, vol 17. CRC Press, New York

Wang C, Zhang T, Guo W (2013) The im mutant gene negatively affects many aspects of fiber quality traits and lint percentage in cotton. Crop Sci 53:27–37

Wang C, Lv Y, Xu W, Zhang T, Guo W (2014) Aberrant phenotype and transcriptome expression during fiber cell wall thickening caused by the mutation of the Im gene in immature fiber (im) mutant in *Gossypium hirsutum* L. BMC Genom 15:94

Xu B, Huang Y (2004) Image analysis for cotton fibers part II: cross-sectional measurements. Text Res J 74:409–416

Zhang H-B, Li Y, Wang B, Chee PW (2008) Recent advances in cotton genomics. Int J Plant Genomics. doi:10.1155/2008/742304

Zhang T et al (2015) Sequencing of allotetraploid cotton (*Gossypium hirsutum* L. acc. TM-1) provides a resource for fiber improvement. Nat Biotechnol 33:531–537